Matrix Creation for Mass-Manufacturing the Microprismatic Plane-Focusing Lenses

Eugene Antonov ⓘ, Minglei Fu ⓘ *, Member, IEEE*, Volodumyr Lysenko ⓘ, Dmytro Manko ⓘ, Viacheslav Petrov ⓘ, and Volodymyr Zenin ⓘ

Abstract—We propose an algorithm for simulating matrix parameters suitable for mass- manufacturing the microprismatic plane-focusing Fresnel lenses. These specialized lenses create a homogeneous light spot at the focus, distinguishing them from traditional point-focusing Fresnel lenses. Incorporating plane-focusing lenses into automatic control systems with four-plane photodetectors enables the formation of linear direction-finding characteristics for moving objects with an expanded bearing angle. In solar photovoltaic modules, these lenses offer optimal solutions for reducing internal ohmic losses, thereby mitigating module overheating caused by sunlight concentration on the module surface. However, plane-focusing lenses are not currently available in optical practice, necessitating their mass production. In this paper the geometrical parameters of our plane-focusing microprism devices are specialized for lens and matrix formation using diamond cutting technique. This facilitates mass manufacturing of the lenses via thermo-pressing method. The simulated lens parameters have been investigated using computer modeling with Solidworks 2016 and TracePro 7.3. Samples of plane-focusing microprismatic lenses were fabricated by thermal pressing of polycarbonate workpieces with a metal stamp-matrix created using our simulation data. The optical characteristics of manufactured lens samples were experimentally tested using a collimated laser beam.

Index Terms—Computer modelling, microprismatic structure, simulating matrix for plane-focusing optics.

I. INTRODUCTION

SOLAR concentrator modules are undergoing now rapid development in many countries [1], [2], [3], [4]. The utilization of concentrator modules offers the possibility to reduce the consumption of semiconductor materials required to generate a specific electrical power, because this reduction is directly proportional to the multiplicity of light concentration within the surface of photovoltaic (PV) modules.

Various studies have been undertaken to improve efficiency and optimize the construction of the lenses for solar concentration. In one study, Ahmadpour A. et al. focused on enhancing the module effectiveness by a Linear Fresnel Reflector Solar Concentrator [5]. This involved curving the primary mirrors slightly to concentrate rays and introducing a novel two-part secondary reflector to redirect received rays to the absorber tube. In a related investigation, the analysis of focal length change was performed through simulation [6]. To address chromatic aberration resulting from the dispersion relationship between the material's refractive index and wavelength, the authors proposed a design, where each Fresnel lens groove are functioning at varied wavelength. Beltagy H. undertook an exploration of new shapes for the secondary reflector in a Fresnel linear concentrator [7]. This study aimed to optimize a solar prototype utilizing Fresnel concentration with a Double Parabolic Concentrator. Modeling of various solar field parameters employed the Monte Carlo ray-tracing method, resulting in the development and commercialization of several thermal power stations based on these optimal configurations. Montanet E. et al. subsequently shifted their focus to studying the influence of the orientation and inclination of solar irradiation on the optical performance of the Linear Fresnel Collector [8]. A ray-tracing model was utilized to evaluate the optical performance for each solar position, and a consistent methodology was developed to assess solar position within the module reference system. Finally, Kiyaee S. et al. introduced a Spectral Splitting Fresnel Lens tailored for linear concentration [9]. This pioneering design selectively directed a specific spectrum portion to the cell while diffracting the remainder, obviating the necessity for beam splitters in spectral splitting solar systems.

Currently, the traditional point-focusing Fresnel lenses are primarily employed for concentrating sunlight in PV modules [10]. High-concentration photovoltaic (HCPV) modules with concentration multiplicities ranging from hundreds to several thousand can be constructed only on the microprismatic Fresnel lenses. However, the non-uniform irradiation distribution on the PV surface in solar HCPV modules with these lenses presents a significant challenge. Increased illumination inhomogeneity across various points of the photocell surface results in elevated side currents within the HCPV structure. Consequently, ohmic losses escalate [10], leading to module overheating. Neo D.W.K. et al. propose an alternative approach to optimizing the overall optical performance of lens arrays in solar concentration modules [11]. By arranging Fresnel lenses in either a rectangular

or hexagonal layout, they aim to maximize sunlight collection, achieving a fill factor of 100% - equivalent to the total area of the module. A high fill factor for Fresnel lens arrays can also be attained using polygonal lenses [12]. While previous attempts with circular trimmed lenses and full polygonal lenses have encountered certain optical drawbacks, the composite polygonal Fresnel lens circumvents these issues through its innovative design. Featuring a radial symmetric Fresnel center filling into a polygon, this design eliminates any intersecting facets within the lens by introducing fillets. In their study, Hayashi N. et al. propose a thin and compact concentrator photovoltaic (CPV) module [13], measuring approximately 20 mm in thickness – roughly one-tenth thinner than conventional CPV modules widely deployed in mega-solar systems. This innovation aims to expand the application scenarios for CPV technology. Micro-solar cells are directly affixed to the lens array to reduce the concentrator's focal length and minimize optical losses resulting from reflection. The optical loss of the lens in this module is approximately 9.0%, a value lower than that of conventional CPV modules equipped with secondary optics. The reduced optical losses enhance the CPV module's energy conversion efficiency, enabling to achieve high performance of solar modules. Sahin F.E. et al. examines the impact of introducing a diffractive surface in the optical path [14]. This optical design offers a cost-effective alternative to other methods, as it can be mass-produced using conventional fabrication techniques. Moreover, the design approach can be applied broadly to various solar concentrator systems, accommodating different cell sizes and geometric concentration ratios. For achieving light spot homogenization at the module surface the utilization of Fresnel-Köhler concentrators proves highly effective [15]. Nevertheless, the complexity associated with this optical technique, involving two distinct lenses, poses a significant barrier to its widespread adoption in solar modules.

Above problems of non-uniform irradiation in solar photo-voltaic modules can be effectively addressed through the application of our plane-focusing lenses. Over the past few years, we have actively developed such optics [16], [17], [18], [19]. Our transforming Fresnel lenses form a uniformly illuminated light circle in the lens focal plane, in contrast to plane-focusing lenses, which concentrate sunlight in the center of the focal image. Replacing point-focusing lenses with our plane-focusing microprismatic optics [18] in the construction of photovoltaic solar modules completely resolves overheating and power loss issues in HCPV modules. Another notable aspect of our plane-focusing optics is their capability to reduce the focal length f of concentrator lenses in photovoltaic modules. For instance, the lens with an optical diameter $D_L = 56$ mm is equivalent to a traditional rectangular lens measuring approximately $\sim$40 x 40 mm [10]. This lens can be manufactured now with reduced focal length $f = 20$–25 mm, compared to the typical values of 75–105 mm [10]. The focal length values f for our transforming lenses [18] is constrained solely by the limit angles $\alpha_{k\ max}$ of refractive microprism zones [20]. Consequently, the reduced f–value contributes to the reduction of concentrator single cell dimensions and the overall thickness of HCPV modules – it is especially crucial factor for space solar applications. Another

application field for plane-focusing Fresnel optics is the automatic control systems equipped with four-plane photodetectors [19]. These lenses facilitate the acquisition of linear direction-finding characteristics for moving objects with an enlarged bearing angle.

Presently, we have fabricated numerous individual samples of plane-focusing lenses based on our simulated lens parameters, utilizing the diamond microcutting technique [21], [22]. This technique ensures the creation of prismatic working facets characterized by exceptional geometrical accuracy and a mirror-like surface quality. Recently, we have successfully employed this method to manufacture microprism structures for computer eye-glasses [23]. Now, each of our plane-focusing lenses has been individually formed through microcutting of plastic workpieces. However, to construct HCPV modules or automatic control systems, hundreds of new lenses are required. Therefore, our algorithm [16], [17], [18], [19] needs to be modified to create a lens design suitable to lens mass replication.

Our paper aims to present an algorithm for simulating lens and matrix parameters suitable to mass manufacturing of new plane-focusing Fresnel lenses using the thermo-pressing method. Additionally, we seek to investigate the calculated lens parameters to optimize their performance through computer modeling with Solidworks 2016 and TracePro 7.3. The samples of stamp-matrixes were formed using the diamond mi-crocutting technique, employing simulated lens parameters, for mass-manufacturing the new transforming lenses. Furthermore, the main properties of manufactured matrixes and lenses for solar concentration modules and control systems applications were experimentally investigated by collimated laser beam to accurately determine the realized geometrical and optical lens parameters.

II. ALGORITHM OF SIMULATING MATRIXES FOR FRESNEL TRANSFORMING OPTICS

In our previous papers [16], [18], [19] an algorithm was proposed for modeling the geometrical parameters of micro-prismatic plane-focusing lenses for light beam transformation. These Fresnel lenses form a light circle of required radius r_V with an almost homogeneous illumination distribution in the focal plane F.

The stamp-matrix used for manufacturing lenses, obviously, should possess a microrelief that mirrors that of the lens itself. The scheme of light refraction for such matrix is shown in Fig. 1, where f is the lens focal distance; n_0 and n_1 are the refractive indices of the medium and the material of lens, accordingly; R_k is the radius of annular prismatic zones $k = 0, 1, 2, 3, \ldots, N$ of the lens; ΔR_k is the width of the refractive k–zone of the lens in the direction of axis X^0; $r_V = R_0$ is the outer radius of the light spot in the focal plane; γ_k is the angle of observation for each k–zone from the focus F; α_k is the prism refractive angle, β_k is the back angle of all microprisms; and h_k is the relief depth for k–zone.

The calculation procedure is similar to the creation of ophthal-mology microprisms [24]. This algorithm for calculating the fo-cusing structure suitable for implementing the diamond-cutting
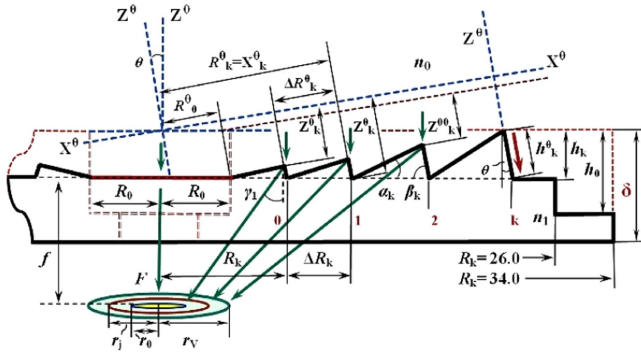
Fig. 1. Scheme of matrix for manufacturing the Fresnel annular focusing structure with variable pitch ΔR_k and depth h_k of microrelief.

method involves, initially, defining of central lens zone, which in the process of lens manufacturing remains flat. The size R_0 of this zone is determined primarily by technological requirements: during diamond-cutting the speed of rotation of the cutting tool at the point $R_0 = 0$ is zero; hence the value of R_0 cannot be zero or very small. A parallel light beam traverses this flat zone of radius R_0 without refraction, resulting in the formation of a flat area with a radius $r_V = R_0$ at the center of the focal plane. All other annular refractive lens zones with inclined flat surfaces of radii R_k and widths ΔR_k should focus the transmitted light onto this single central circle of radius r_V at the lens focal plane.

All subsequent stages of modeling process for lens parameters are thoroughly detailed in our paper [18]. When simulating matrix parameters, the initial step is to determine the technology by which this matrix will be formed. The process of diamond microcutting of a plane metal workpiece with a thickness of δ (Fig. 1) it is advisable to start from the central zones of the matrix with minimum R_k value (point "0" in Fig. 1). In this case, the microchip from the cutter at any radius R_k will not spoil the already created annular optical surface with the width $\Delta R_k = R_{k+1} - R_k$ at the matrix radius R_{k+1}, thus ensuring the maximum cleanliness of created working surfaces of microrelief.

During lens manufacturing using the thermo-pressing technique, the inclination angle of microprisms θ (Fig. 1) is very important. Based at our previous experience in manufacturing the ophthalmology microprisms [24] this angle θ should be set at approximately 3–4 degrees. This facilitates easier separation of the metal stamp-matrix from the formed plastic lenses at the end of thermo-pressing process. Consequently, the prism back angle β_k should be reduced to value $(90-\theta)$ degrees. The diamond cutter tool while matrix formation is moving in the direction Z_θ. The brown arrow in Fig. 1 indicates the direction of movement of the tool for this specific case. To achieve the desired angle β_k this Z_θ axis should be inclined to designated value of θ relative to Z_0 axis, which is perpendicular to the forming surface of the workpiece. The depths h_k of all matrix k–zones should have the same value, but with different back angles $\beta_k = (90-\theta)$ degrees to form the necessary refractive angles α_k of the lens.

The central flat part of the matrix cannot be formed using diamond cutting due to the impossibility of aligning the cutter parallel to X_0 axis in this zone, which is buried by the depth

$h_{k\ max}$ relative to the forming surface of the workpiece. So, this central zone is formed using a different technique – by drilling the hole with a small fixing shoulder of diameter R_0, followed by the installation of a special pin with a polished top end of the same diameter R_0, placed at the necessary depth $h_{k\ max}$. Similarly, the periphery part of the matrix also should have a special configuration to form the lens of necessary light diameter D_L with the mouth of proper depth h_0, which is necessary for facilitating the thermo-pressing process.

III. NUMERICAL ANALYSIS OF THE SIMULATED MATRIX STRUCTURE

Let us consider the creation of matrix #05c1m for mass-manufacturing the lenses with inclination angle $\theta = 3$ degrees, focus $f = 41$ mm and light diameter $D_L = 50$ mm, which form the focal homogeneous spot of radius $r_V = 4.5$ mm. Such lens is necessary for certain real automatic control system with four-plane photo-detector of round working area of diameter $D_D = 9.0$ mm. Initially, we will focus on simulating the parameters of lens #05c1, as our algorithm for matrix simulation requires knowledge of all lens parameters: zone radii R_k, relief depths h_k and prism refractive angles α_k.

Radius of "dark" central area of lens focal image is selected as $r_0 = 0.4$ mm, which is the optimal one according to our previous data [16], [17], [18], [19]. The pitch correction process [18] realizes the lens structure of 6 prismatic zones labeled as #1–6. The calculated values of lens zone correction $\Delta R'_k$ [18] are illustrated in Fig. 2(a), while the scheme of focusing optimization FO [18] is depicted in Fig. 2(b). We denote this focusing scheme FO = 0.4-0.4-1.0-1.8-2.5-3.3. Prismatic zones #1–2 reflect light beams to the focal light ring of width $W_1 = r_V$-$r_0 = 4.1$ mm, zone #3 – to the ring of $W_2 = r_V$-$r_1 = 3.5$ mm, zone #4 – to the ring of $W_3 = r_V$-$r_2 = 2.7$ mm, zone #5 – to the ring of $W_4 = r_V$-$r_3 = 2.0$ mm and zone #6 reflect light beams to the ring of $W_5 = r_V$-$r_4 = 1.2$ mm. Under above conditions the focal light spot has the "dark" area of radius $r_0 = 0.4$ mm and five light peaks $(M = 5)$ for $r_j = 0.4; 1.0; 1.8; 2.5; 3.3$ mm with outer radii $r_V = 4.5$ mm.

The calculated enlargement of prismatic zones appears considerably larger compared to the nominal pitches $W_j = r_V$-r_j (Fig. 2(a)). Consequently, considering the future diamond cutting process for lens manufacturing, zone #1 of the lens #05c1 up to radius $R_5 = 8.672$ mm should be composed of 5 separate prismatic element (see Fig. 3); zone # 2 extending to $R_{13} = 13.063$ mm – from 8 identical microprisms; refractive zones # 3-4 extending to $R_{22} = 17.081$ mm and $R_{31} = 20.426$ mm, respectively – each from 9 separate prismatic elements; zone # 5 extending to $R_{39} = 23.100$ mm – from 8 identical microprisms; and zone # 6 extending to $R_{44} = 24.809$ mm should be made from 5 separate prismatic elements. In this scenario, all widths ΔR_k of prismatic zones less than 0.85 mm enabling the simulated lens profile to be realized via diamond cutting technique [21], [22], [23], [23].

Lens parameter simulation was conducted for polycarbonate $(n_1 = 1.564)$ for wavelength $\lambda = 1.064\ \mu$m, considering that just infrared illumination of moving objects is commonly used
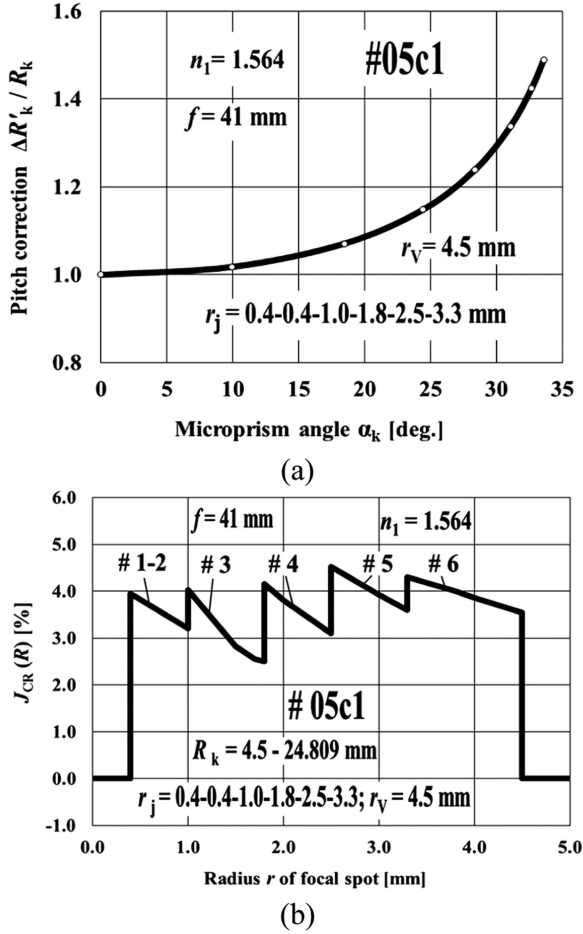
(a)

(b)

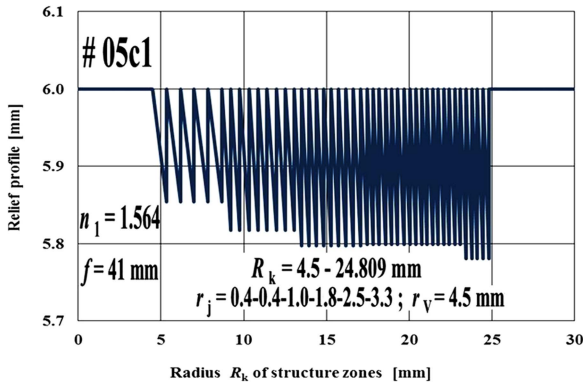Fig. 2.   (a) Pitch correction; (b) Scheme of focusing optimization for lens #05c1.

Fig. 3.   Structure of microrelief of lens #05c1 with $D_L = 50$ mm and focus of $f = 41$ mm, which forms a focal light spot of radius $r_V = 4.5$ mm.

in automatic control systems. The refractive indices $n_1(\lambda)$ were used from the available data [25]. The calculated relief structure for the lens-concentrator # 05c1 with $R_{k\ max} = 24.8$ mm is shown in Fig. 3. The prismatic profile for all lens zones was simulated with approximately the same relief depth h_k ranging from 150 to 220 μm to simplify the future process of thermo-pressing.

The simulated matrix structure, evidently, possesses a reverse profile compared to the lens profile. Matrix profile can be easily calculated using obtained table data on lens parameters: R_k, h_k and α_k. Both simulated datasets were utilized for the practical manufacture of lens #05c1 and stamp-matrix #05c1m.

In the traditional manufacturing process outlined in our algorithm [16], [17], [18], [19], the lenses are individually manufactured with a prism inclination angle $\theta = 0$ degrees, measured between the reverse facet of all formed microprisms and the plane, orthogonal to the relief forming plate. During manufacturing, the diamond cutter moves along the axis X^0 (see Fig. 1), shaping the prism working surfaces with widths ΔR_k. This axis, perpendicular to the relief forming plate's rotation plane to the direction Z^0, dictates the relief depths h_k. Consequently, the back angle of all microprisms created within the lens remains fixed at $\beta_k = 90$ degrees.

For matrix #05c1m formation the inclination angle θ should be changed to value $\theta = 3.0$ degrees. So, we have to set all microrelief radii ΔR_k, depths h_k and prism back angles β_k in this new coordinate system (X^θ, Z^θ) that should be turned to this angle θ relative to coordinate system (X^0, Z^0). These new values of ΔR^θ_k, h^θ_k and β^θ_k can be obtained as following:

$$\Delta X^\theta_k = \Delta R^\theta_k = \Delta R_k \cos\theta + (h_k - h_{k-1})\sin\theta \quad (1)$$

$$\beta^\theta_k = 90 - \theta \quad (2)$$

$$\Delta Z^\theta_k = h^\theta_k = h_k / \cos\theta \quad (3)$$

We have decided to start the cutting tool movement at the point "0" (see Fig. 1). So, our calculations also should be connected with this initial point. Because the angle θ for relief forming plate inclination relative to axis X^0 in coordinate system (X^0, Z^0) is the non-zero one, the distances accumulation takes place in values ΔR^θ_k and h^θ_k along the axis (X^θ, Z^θ):

$$X^\theta_k = \Sigma\Delta X^\theta_k = \Sigma\Delta R^\theta_{k+1} \quad (4)$$

$$Z^\theta_k = h^\theta_k + \Sigma\Delta R^\theta_{k+1} tg\theta \quad (5)$$

The data on X^θ_k and Z^θ_k obtained by formulas (1)–(5) for manufacturing the lens #05c1 with inclination angle $\theta = 3.0$ degrees are shown in Fig. 4(a). Fig. 4(b) illustrates the similar data for the case of matrix #05c1m manufacturing. Obtained values of X^θ_k and Z^θ_k allow totally organize the movement of cartridge with diamond cutter tool along the axis (X^θ, Z^θ).

Similar data on X^θ_k, Z^θ_k and β^θ_k can be early obtained by proposed algorithm for others lens diameters D_L and focal lengths f, as well as for another plastic material – silicon or polymetilmetacrylat, from which the lenses usually are made for HCPV solar concentration modules [2], [10] and for automatic control systems [19].

IV. COMPUTER MODELLING OF TRANSFORMING LENSES

A notable observation across all focal light spot profilograms for all investigated lenses [16], [17], [18], [19], analyzed using *Image-J 1.53* software [26], is a noticeable expansion of the profiles beyond the calculated values. Consequently, the primary objective of our computer modeling was to explore the
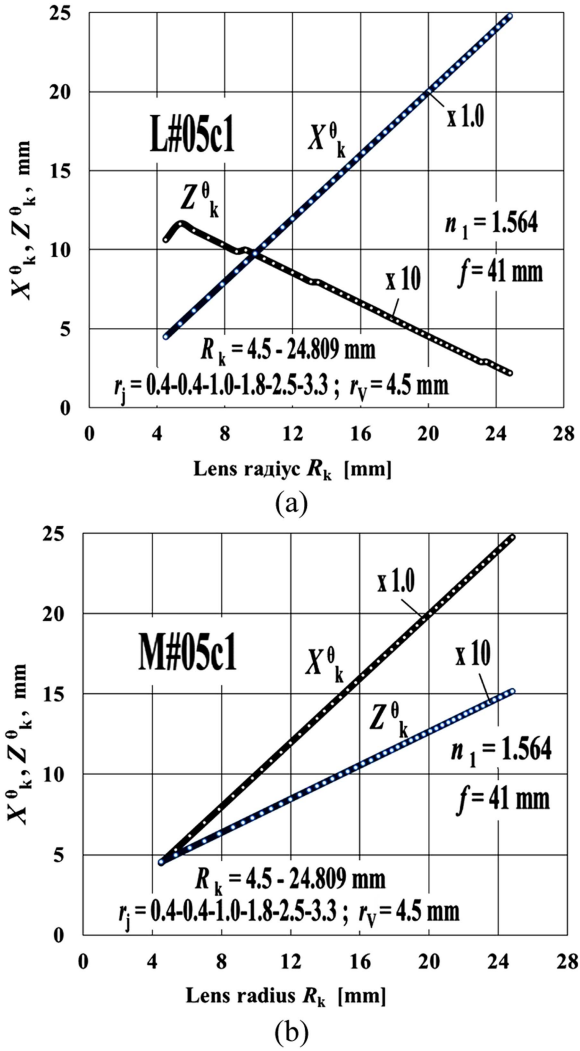
(a)

(b)

Fig. 5. Computer model of lens #05c1 (a); laser beam passing through lens model, 1% of beams, red color – 66-99 % of initial beam intensity, blue color – 0-33 % of initial beam intensity (b).

(a)

(b)

Fig. 4. Calculated distances X^{θ}_k and Z^{θ}_k for manufacturing structure #05c1: (a) lens manufacturing; (b) matrix manufacturing.

underlying causes behind this expansion, using the calculated geometrical parameters for lens #05c1.

In the initial modeling phase, we employed the *Solidworks 2016* software [27] to generate a computer model of lens #05c1 (see Fig. 5(a)). Subsequently, this created lens model was imported into the *TracePro 7.3* software [28] for further modeling of the rays passing through the lens #05c1 employing geometric optics approximation via the Monte Carlo method.

The light source comprised a parallel beam of rays, uniformly distributed in the direction perpendicular to the lens plane. The scheme of total beam trajectory through the lens #05c1 as simulated in the *TracePro 7.3* program is shown in Fig. 5(b): incident and refracted rays with the intensity of 66–99 % of the incident ones are marked in red color, refracted and reflected rays with an intensity of 0–33% – in blue. The screen was a cylinder with a diameter $d_E = 50$ mm, positioned at the distance $f = 41$ mm from the relief surface of the lens (shown in green).

The profile of the focal light spot for lens #05c1, as obtained experimentally using collimated laser beam, is shown in Fig. 6(a); the simulated profile from the *TracePro 7.3* software
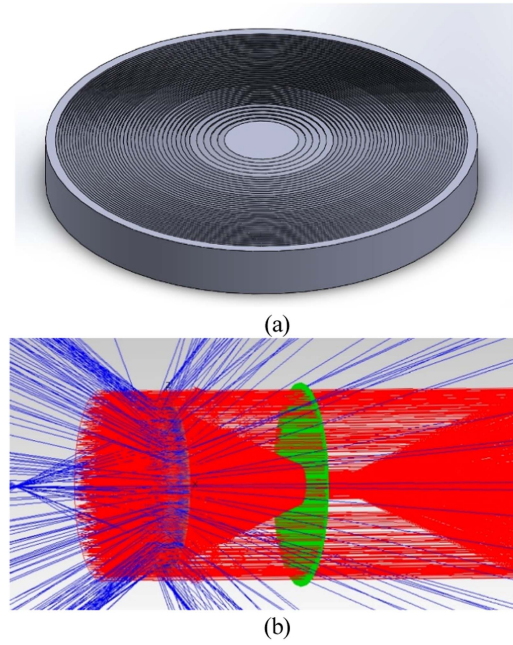
for transmitted light flux for observation distance $f = 41$ mm is shown in Fig. 6(b). The large central light maximum corresponds to the refracted laser beam transformed by the lens. The smaller light peaks at the periphery are non-refracted collimated laser beam passed outside the lens. Dotted lines indicate calculated profile width: 200 pixels (Fig. 6(a)) ≈ 9.5 mm (Fig. 6(b)). Notably, a close correspondence is observed between the practical results obtained through simulation and experimentation. The *TracePro 7.3* profile (Fig. 6(b)) aligns better with the calculated distribution of passed light intensities (Fig. 2(b)) compared to experimentally determined profile (Fig. 6(a)). This observation may be attributed to the absence of diffuse light ray scattering on relief defects and the exclusion of diffraction phenomenon [20] during computer modeling.

However, in both instances the actual profiles display a noticeable expansion, extending to values of $r = 6$–7 mm within the designated area of $r_V = 4.5$ mm. This observed extension prompts a comprehensive exploration into the contributing factors and underlying mechanisms influencing the broader spatial distribution of the intensity.

To investigate this phenomenon, the path of light rays through the individual zones #1–6 of lens #05c1 was simulated using the *TracePro 7.3* software. Obtained data are shown in Fig. 7, depicting each of the lens zones #1–6. In Fig. 7(a), shaded areas represent the simulated profile expansion zone of $r_V^M = (4.5$–6.0) mm; solid black line in in Fig. 7(b) denotes the total expansion effect for all zones #1–6. Dotted lines indicate the width of designated focal spot of radius $r_V^C = 4.5$ mm. The colors of curves for zones #1–6 are consistent across both Fig. 7(a) and (b).

The data showed that the radius of "dark" area r_j^M in the center for all simulated images of outer radius $r_V^M = 4.5$ mm
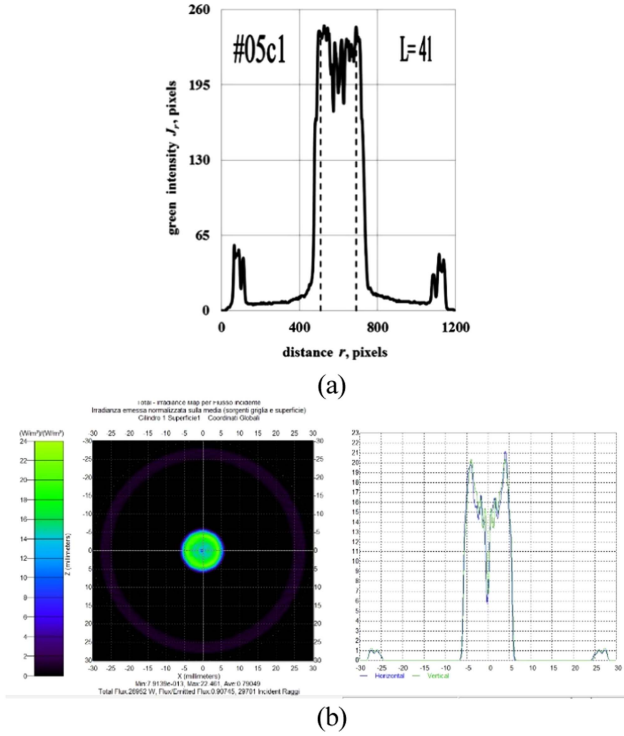
(a)

(b)

Fig. 6. Profile of transmitted light beam in the focal plane for lens #05c1 of light diameter $D_L = 50$ mm and focus length $f = 41$ mm: (a) experimental profile; (b) computer modeling: 200 pixels ≈ 9.5 mm.

corresponds roughly to our calculated data (Fig. 2(b)) and varies from value $r_j^M = 0.6$ mm (zones #1–2, calculated value $r_j^C = 0.4$ mm); to $r_j^M = 1.2$ (zone #3, $r_j^C = 1.0$ mm), to $r_j^M = 2.3$ (zone #4, $r_j^C = 1.8$ mm), to $r_j^M = 2.9$ (zone #5, $r_j^C = 2.5$ mm) and to $r_j^M = 4.0$ mm (zone #6, $r_j^C = 3.3$ mm). The total simulated light flux for all zones of lens #05c1 (Fig. 7(b), black curve) exactly corresponds to the sum intensities for separate prismatic lens zones #1–6, that is good evidence for fine accuracy of created model for computer modeling.

However, the expansion of profiles is obvious compared to designated value $r_V^C = 4.5$ mm, especially for peripheral lens zones #4–6, and varies from radius $r_V^M = 5.2$ mm (zone #1) to $r_V^M = 5.5$ mm (zone #2), to $r_V^M = 5.9$ (zone #3), to $r_V^M = 6.1$ (zone #4), to $r_V^M = 6.2$ (zone #5) and to radius $r_V^M = 6.4$ mm (zone #6). So, the expansion of beam profiles for lens #05c1 really exists, a reason for this effect is not connected with the diffraction phenomenon and the diffuse scattering of laser rays on microrelief defects, which were not included in our computer modeling. This effect also is increasing with the increase of refraction angle α_k from the center to periphery zones of the lens (Fig. 8, "blue" rays).

Subsequent computer modeling proved (see Fig. 9) that expanded final light beam is formed due to additional reflection of incident laser rays from the inner surface of the refractive prismatic surfaces of the lens, followed by their refraction of inner surface of lens forming plate. Consequently, an additional light beam is formed from these additionally refracted "blue" rays with an intensity of (0–10) % (shown in Fig. 9(a) in blue color). This phenomenon is responsible for the total expansion
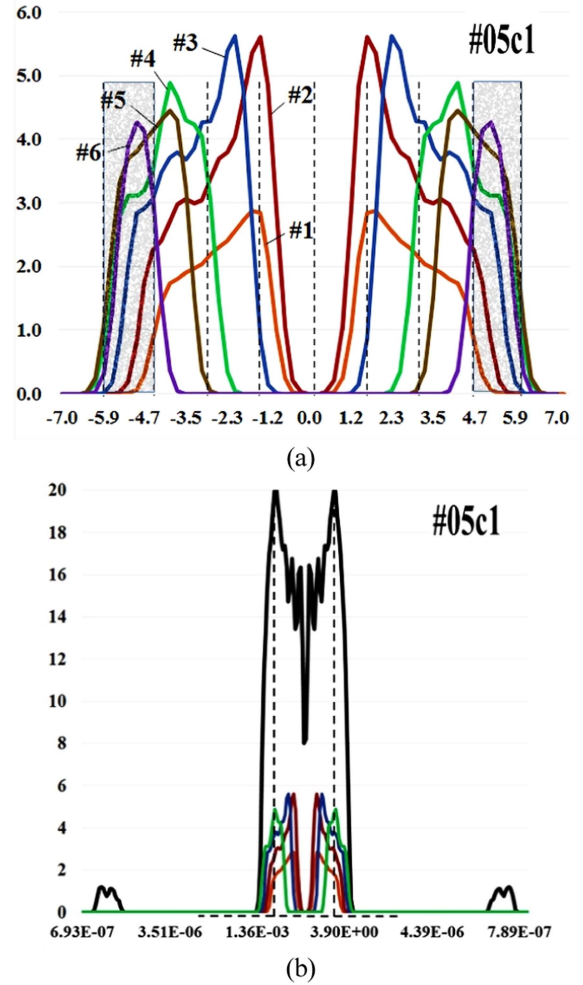

(a)

(b)

Fig. 7. Computer modeling of transmitted light fluxes for lens #05c1: (a) rays for separate prismatic zones #1-6; (b) total laser beam for zones #1-6.

of refracted light (Fig. 9(b)) of intensity (0–66) % (depicted in blue-green).

The data shown in Fig. 9 were obtained for "solar" lens #27 [29] with similar light diameter $D_L = 50$ mm, but with diminished radius $r_V = 1.5$ mm and focal distance $f = 25$ mm, which provides the larger beam expansion effect due to the larger values of refracted angles α_k comparing to similar refractive zones of lens #05c1 with focus $f = 41$ mm.

Based on our computer modeling, the value of laser beam expansion for lens #05c1 ranges from 1.2 to 2.0 mm, aligning closely with experimental data, taken from laser diagnostics. The peripheral zones contribute significantly to the overall optical behavior, showcasing their pivotal role in shaping lens focusing properties. The observed expansion of focal spot profiles for plane-focusing lenses primarily stems from the phenomenon of internal reflection of transmitted laser beams, particularly pronounced for peripheral zones.
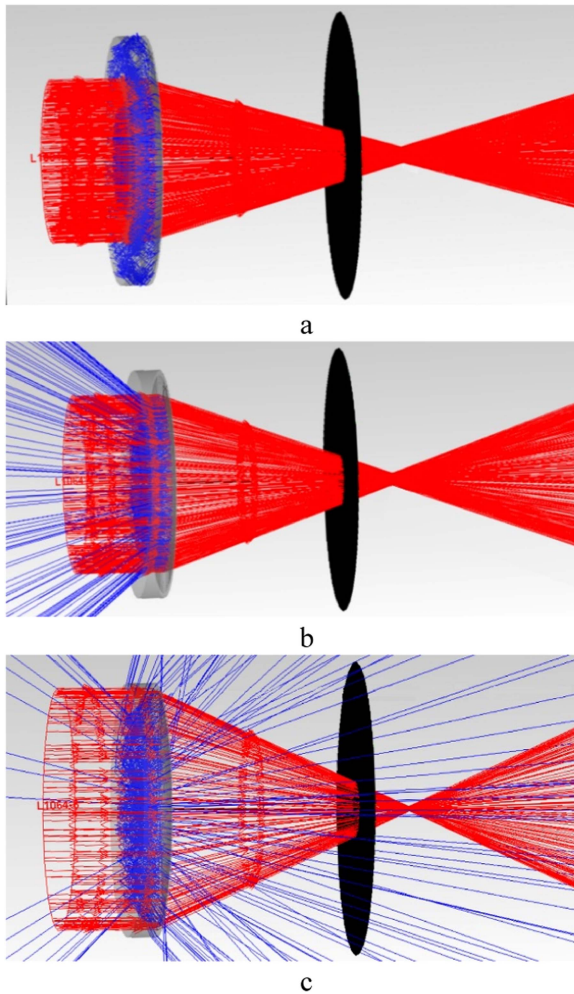
Fig. 8. Light beams passing lens #05c1, 5% rays: (a) zone #3; (b) zone #4, (c) zone #6: refracted light rays with intensity (0-33) % - in blue; (66-99) % - in red color).
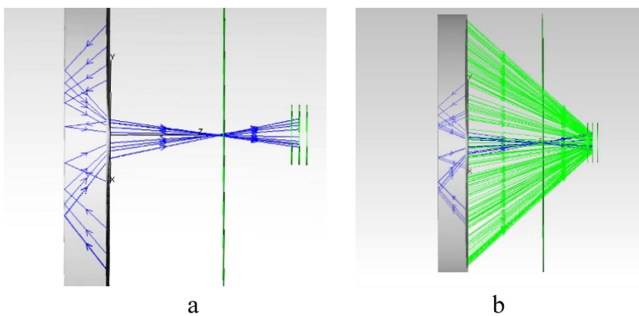

Fig. 9. Scheme of formatting additional light beam in center region of main beam for lens #27: (a) intensity (0-10) % of incident light beam (in blue); (b) refracted light beam of intensity (0-66) % (in blue-green).

V. MANUFACTURE OF MICROPRISMATIC LENSES BY DIAMOND MICROCUTTING

A well-established optical production technology, used for crafting various lenses, is ultra-precision machining (UPM) [21], [22]. Method UPM using a diamond tool enables the creation of lenses with exceptional geometrical accuracy and mirror-like surfaces. Such lenses meet the highest needs of optical industry.
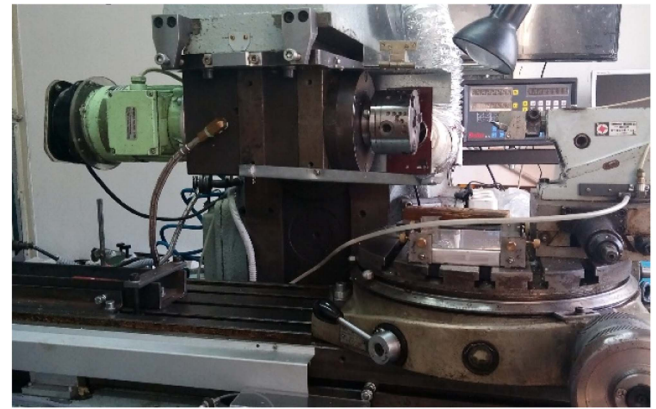

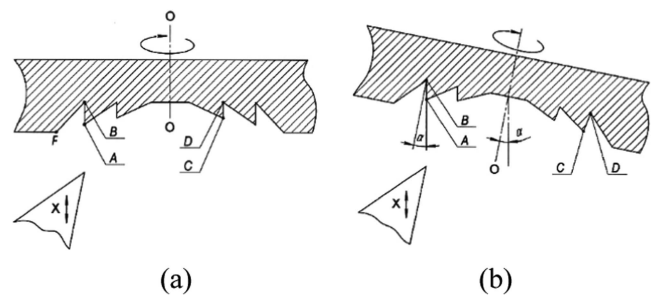Fig. 10. Front view of experimental DMC installation of IIR.

Fig. 11. Scheme for formation of circular microrelief of matrix: (a) angle of inclination of matrix workpiece $\alpha = 0$ degrees; (b) angle $\alpha > 0$ deg.

This technology involves direct diamond cutting guided by computer control, facilitating precise tool movement along desired surface features.

Similar technology, referred to as diamond microcutting (DMC), has been effectively developed [19], [23] in the Institute for Information Recording of National academy of Sciences of Ukraine (IIR) to manufacture our simulated microprisms. The general view of our microcutting installation is shown in Fig. 10. A diamond cutter tool is housed in a special cartridge, enabling the movement of this cartridge with the diamond cutter of cutting angle α_G along (X, Z) axis with calculated clearance angle ζ. Computer control allows setting the necessary cutter positions in this coordinate system by few micrometers accuracy (no more ~5 μm). Diamond cutter for shaping relief of simulated lens #05c1 has almost similar to parameters [22]: nose radius $r_N = 10 \,\mu$m, rake angle $\alpha_G = 46$ degrees, clearance angle ζ is changed from 5 to 40 degrees and opening angle $\alpha_0 = 86$ degrees.

For practical implementation of our simulated design for plane-focusing optics, suitable for their mass production using thermo-pressing method, the initial step involved modernizing the DMC machine 6P82 type, utilized in IRR [23] for forming the circular microrelief.

Possible schemes for microcutting the matrix relief are shown in Fig. 11. The metal matrix workpiece is installed in the spindle chuck, which rotates around its "0-0" central axis. In the first option (Fig. 11(a)), the diamond cutter moves along the X_0 axis, forming a corresponding microrelief groove. The faces *AB* and *DC* of the groove are the side non-working cylindrical

surfaces of the microprism, which are vertical to the horizontal forming surface of the workpiece. The number of individual relief grooves is usually up to several dozen.

When forming the final plastic lenses using a matrix with such geometry, at the end of thermo-pressing cycle, when the "matrix-lens" system is cooled, the cylindrical elements of the metal matrix are tightly compressed by the lens polymer due to the difference in the coefficients of linear expansion of the metal and the polymer. Consequently, significant force is needed to separate the manufactured lens from the matrix, posing a risk of damaging the working inclined surfaces of the lens.

To mitigate the force required for separation the lens from the matrix, it was imperative to introduce lateral non-working surfaces on both the lens and the matrix, inclined at stated angle α (as shown in Fig. 11(b)), thereby transforming the cylindrical surfaces AB and DC into the conical ones. Consequently, the forming surface AB should be oriented at an angle α relative to the axis "0-0".

The creation of such conical surfaces at the matrix using IIR machine of 6P82 type under the existing kinematics of spindle movement can be realized in two ways: by turning on necessary angle α the support X with a diamond cutter, or by turning the spindle block with the matrix workpiece. It appears that the turning of support X was more complicated due to many important adjustments necessary to organize the movement of support X of 6P82 machine. Consequently, the modernization was executed by constructing the special turning mechanism for the spindle block of this machine to the required angle α relative to the direction X_0 of diamond tool movement. The precise control of this angle α is performed by specially constructed graduated scale and indicator with the accuracy of ± 1.0 angular minutes.

The modernized spindle block of machine 6P82, equipped with metal matrix workpiece and diamond cutter tool, is shown in Fig. 12(a). The general view of lens #05c1, manufactured by the diamond cutting technique using above spindle is shown in Fig. 12(b).

Experimental investigation of this lens #05c1 was conducted using our specialized laser setup, employing a collimated laser beam of wavelength $\lambda = 0.532$ μm and beam diameter $D_S = 60$ mm. The optical scheme of our experimental setup is discussed in detail in [18]. The obtained data have demonstrated, that the focal light distribution for this lens is practically flat (see Fig. 13). It means that simulated matrix data satisfy the stated task on matrix fabrication. However, it's noted that these profiles, obtained with *Image-J 1.53* software [26], exhibit a slight dependency on the observation distance L, and they are expanded relative to the calculated widths (illustrated by the dotted lines).

During laser investigation of lens #05c1, designed for wavelength $\lambda = 1.064$ μm, with a laser beam with wavelength $\lambda = 0.532$ μm, the appropriate correction Δf_2 of nominal focal distance f_0 should be taken into account [29]. In this scenario, the laser rays are refracted at larger angles γ compared to the calculated values γ_0 and nominal focus distance f_0 is diminishing. This correction value $\Delta f_2 = (f_0 \text{-} f_2)$ increases with the increase of prismatic angle α_k.
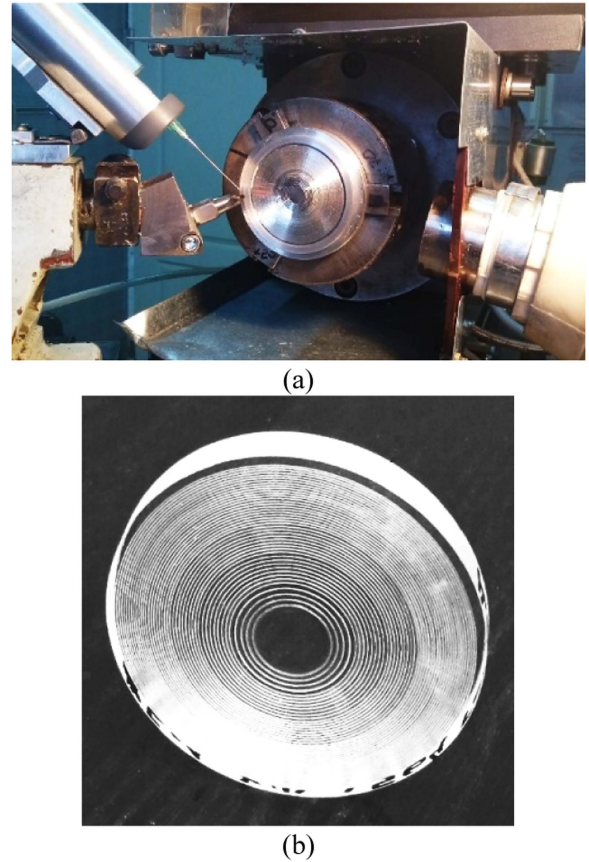

(a)

(b)

Fig. 12. Modernized spindle block of IIR experimental DMC machine (a); general view of lens #05c1 (b).

The calculated diminishing of Δf_2 value [29] for this situation, depending on the refractive angle α_k for lenses with different nominal focal distances f_0, are shown in Fig. 14(a)(solid lines). It's evident that due to this dependency, "green" laser diagnostics cannot accurately determine the efficiency of "infrared" lenses, because the correction value Δf_2 varies across different prismatic zones of the lens. Refracted rays from different lens zones do not converge in a single focus plane. However, such data allow for a certain comparison of lens focusing properties, calculated for "infrared" lenses, and experimental ones, determined with a "green" laser.

The calculated diminishing values Δf_2 for nominal distances f_0=20 and 41 mm for diagnosing "infrared" lenses with "red" laser of wavelength $\lambda = 0.640$ μm are shown in Fig. 14(a) by dotted lines.

Similar correction values Δf_2, calculated for diagnosing "green" lenses with $\lambda = 0.585$ μm ($n_1 = 1.585$) and "infrared" lenses with $\lambda = 1.064$ μm ($n_1 = 1.564$) by "red" laser with wavelength $\lambda = 0.640$ μm ($n_1 = 1.580$), are shown in Fig. 14(b) by solid and dotted lines, respectively.

Using our simulation data, the matrix prototype #05c1m we manufactured the matrix prototype #05c1m from optical polycarbonate by diamond DMC technique. This prototype serves as a lens, when the passing of laser rays is reversed (from the relief side), allowing investigation into the structure and quality of lens prismatic zones. The general view of polycarbonate matrix
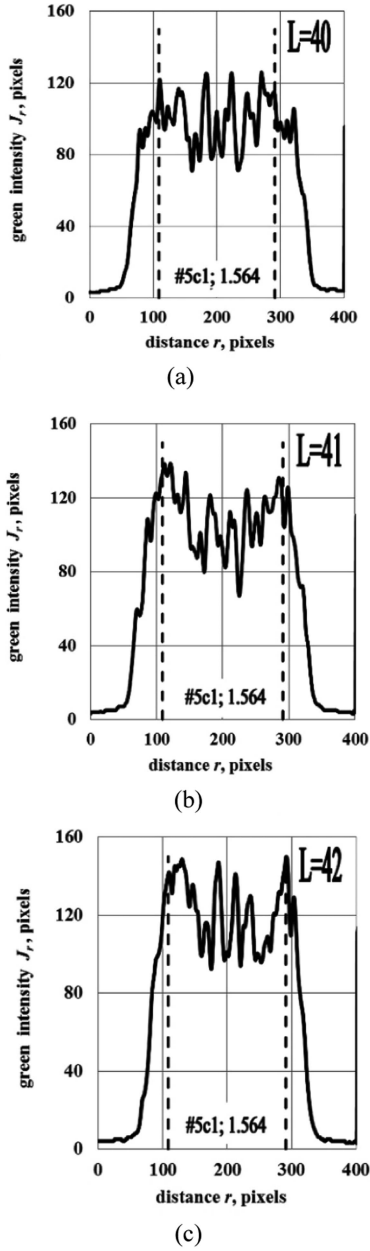
(a)

(b)

(c)

Fig. 13. Profiles of focal light spots for lens #05c1 for different observation distances L: (a) $L = 40$ mm, (b) 41 mm, (c) 42 mm.

(a)

(b)

Fig. 14. Correction values Δf_2 for nominal focal distances $f_0 = 15$-41 mm: (a)– investigating "infrared' lenses by "green" laser (solid lines) and by "red" laser (dotted lines); (b)– investigating "green' lenses (solid lines) and "infrared" lenses (dotted lines) by "red" laser ($\lambda = 0.640$ μm ($n_1 = 1.580$).

(a) (b)

Fig. 15. Image of matrix prototype #05c1 made from PC (a); light image for reverse beam pass for this matrix prototype for distance $f = 41$ mm (b).

prototype #05c1m is illustrated in Fig. 15(a). The functioning of individual zones of lens #05c1m under the reverse path of the rays for nominal observation distance $L = 41$ mm is illustrated in Fig. 15(b). The outer bright light ring represents the collimated laser beam passed outside the lens; while the central bright circle depicts the laser beam passing through the flat central zone of the lens. Obtained data indicate that the structure of refracted beams aligns perfectly with simulated lens geometry; the optical quality of prismatic zones for manufactured structure meets our highest expectations.

The real matrix #05c1m also has been manufactured according to our simulation data. The total view of this matrix #05c1m, made from a special aluminum alloy *W-95*, is illustrated in
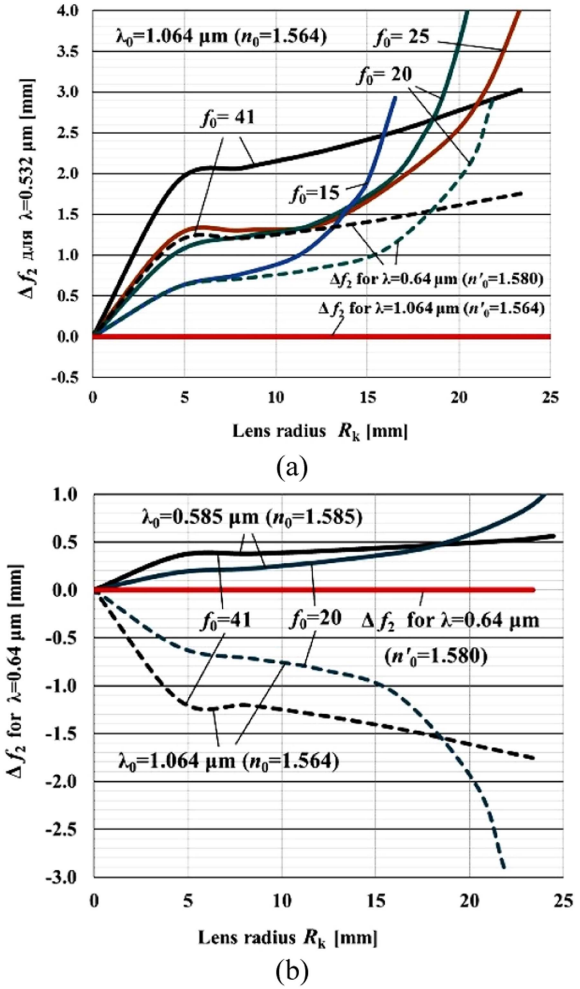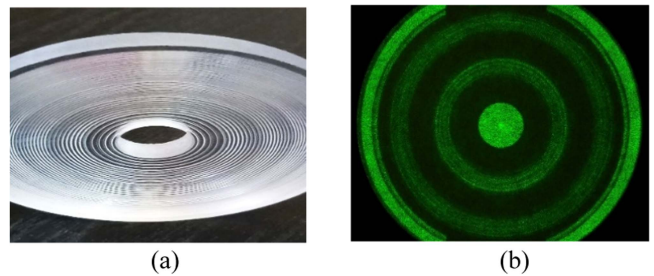
Fig. 16(a). The focal image of transformed light in collimated laser beam of diameter $D_S = 60$ mm for plane-focusing lens #05c1m-02, made from polycarbonate workpiece by thermo-pressing with manufactured metal matrix #05c1m, is shown in Fig. 16(b).

The profiles of focal images for lens #05c1, made individually by diamond cutting from polycarbonate workpiece, and profile for lens #05c1m-02, made with manufactured metal matrix by
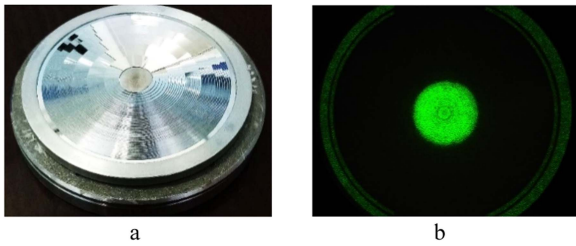
Fig. 16. General view of manufactured metal matrix #05c1m (a) and light image in the focal plane (b) for lens #05c1m-02 of light diameter $D_L = 50$ mm and focus length $f = 41$ mm.
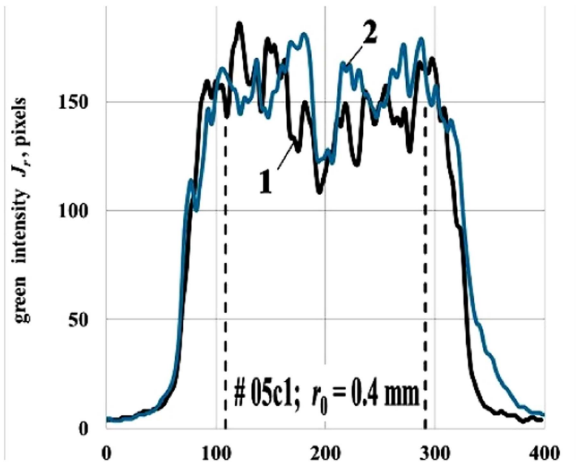

Fig. 17. Profiles of focal light spots for lens #05c1 for observation distances $L' = 40$ mm: 1– lens #05c1; 2– lens #05c1m-02.

thermo-pressing technique, are shown in Fig. 17. These profiles are almost identical.

Both profiles of the focal light spot in Fig. 17(solid lines) exhibit noticeable expansion compared to the calculated profile (dotted lines), attributed to internal reflection of transmitted laser rays, particularly for peripheral lens zones. However, lens #05c1m-02, manufactured using the metal matrix #05c1m, demonstrates highly acceptable focusing characteristics. Experimentally obtained lens parameters aligning perfectly with simulated ones.

Data obtained underscore the feasibility of mass-manufacture of high-quality plane-focusing lenses using metal matrix. These lenses are suitable for both automatic control systems and solar photovoltaic modules, when the homogeneous distribution of image illumination in the lens focus is necessary to achieve the optimum working characteristics of these devices.

VI. CONCLUSION

The algorithm of mathematical simulation was developed and appropriate calculations were performed for creation of plane-focusing microprismatic lenses and matrixes, transforming the refracted light beams into a uniformly illuminated light circle in the lens focal plane. The geometrical parameters of the lenses are adopted for mass manufacturing lenses by thermo-pressing method.

Based on our simulation results, matrixes for the transforming lens-concentrators were manufactured from aluminum alloy W-95 using diamond micro-cutting technique. With these matrixes the samples of high-quality lenses were made by thermo-pressing the flat polycarbonate workpieces. Experimental studies on the optical and lighting characteristics of manufactured lenses demonstrated complete alignment of obtained experimental data with theoretical parameters of the lenses.

Proposed specialized plane-focusing lens-concentrators offer effective alternatives to traditional point-focusing Fresnel lenses in optical concentration photovoltaic modules for diminishing thermal and ohmic losses in the module. Such lenses are also optimal for constructing the automatic control systems with four-plane photodetectors to obtain the linear direction-finding characteristics of moving objects with enlarged bearing angles.

REFERENCES

[1] X. Ju, P. X, Z. Zhang, C. Xu, and G. Wei, "Thermal and electrical performance of the dense-array concentrating photovoltaic (DA-CPV) system under non-uniform illumination," *Appl. Energy*, vol. 250, pp. 904–915, 2019, doi: 10.1016/j.apenergy.2019.05.083.

[2] M. Yamaguchi and A. Luque, "High efficiency and high concentration in photovoltaics," *IEEE Trans. Electron Devices*, vol. 46, no. 10, pp. 2139–2144, Oct. 1999, doi: 10.1109/16.792009.

[3] H. Baig, K. C. Heasman, and T. K. Mallick, "Nonuniform illumination in concentrating solar cells," *Renewable Sustain. Energy Rev.*, vol. 16, pp. 5890–5909, 2012, doi: 10.1016/j.rser.2012.06.020.

[4] P. Benitez et al., "High performance Fresnel-based photovoltaic concentrator," *Opt. Exp.*, vol. 18, no. S1, pp. A25–A40, 2010, doi: 10.1364/OE.18.000A25.

[5] A. Ahmadpour, A. Dejamkhooy, and H. Shayeghi, "Optimization and modelling of linear Fresnel reflector solar concentrator using various methods based on monte carlo ray–trace," *Sol. Energy*, vol. 245, pp. 67–79, 2022, doi: 10.1016/j.solener.2022.09.006.

[6] C. Y. Bachhav and P. D. Sonawwanay, "Study on design and performance enhancement of Fresnel lens solar concentrator," *Mater. Today: Proc.*, vol. 56, no. Part 5, pp. 2873–2879, 2022, doi: 10.1016/j.matpr.2021.10.168.

[7] H. Beltagy, "A secondary reflector geometry optimization of a Fresnel type solar concentrator," *Energy Convers. Manage.*, vol. 284, 2023, Art. no. 116974, doi: 10.1016/j.encnman.2023.116974.

[8] E. Montanet, S. Rodat, Q. Falcoz, and F. Roget, "Influence of topography on the optical performances of a Fresnel linear asymmetrical concentrator array: The case of the ELLO solar power plant," *Energy*, vol. 274, 2023, Art. no. 127310, doi: 10.1016/j.energy.2023.127310.

[9] S. Kiyaee, S. Ya., and A. Z. Moshfegh, "A new designed linear Fresnel lens solar concentrator based on spectral splitting for passive cooling of solar cells," *Energy Convers. Manage.*, vol. 230, 2021, Art. no. 113782, doi: 10.1016/j.enconman.2020.113782.

[10] V. D. Rumyantsev et al., "CPV modules based on lens panels," *Adv. Sci. Technol.*, vol. 74, pp. 211–218, 2010, doi: 10.4028/www.scientific.net/AST.74.211.

[11] D. W. K. Neo, A. S. Kumar, and M. Rahman, "An automated Guilloche machining technique for the fabrication of polygonal Fresnel lens array," *Precis. Eng.*, vol. 41, pp. 55–62, 2015.

[12] N. Y. J. Tan, Z. H. Lim, G. G. Zhou, K. Liu, and A. S. Kumar, "Design and fabrication of composite polygonal Fresnel lenses," *Opt. Exp.*, vol. 29, no. 22, 2021, Art. no. 436290, doi: 10.1364/OE.436290.

[13] N. Hayashi et al., "High-efficiency thin and compact concentrator photovoltaics with micro-solar cells directly attached to a lens array," *Opt. Exp.*, vol. 23, no. 11. pp. A594–A602, 2015, doi: 10.1364/OE.23.00A594.

[14] F. E. Sahin and M. Yılmaz, "High concentration photovoltaics (HCPV) with diffractive secondary optical elements," *Photonics*, vol. 6, no. 68, 2019, Art. no. 23562, doi: 10.3390/photonics6020068.

[15] P. Zamora et al., "Experimental characterization of fresnel-köhler concentrators," *J. Photon. Energy*, vol. 2, pp. 1–12, 2012.

[16] E. E. Antonov, M. L. Fu, V. V. Petrov, M. D.Yu., and K. H. Rong, "Structure of microprismatic fresnel lenses for creating uniform focal images," *Opt. Exp.*, vol. 29, no. 24, pp. 38958–38970, 2021, doi: 10.1364/OE.438590.

[17] M. L. Fu, E. E. Antonov, M. D. Yu, V. V. Petrov, and K. Z. Rong, "Microprismatic fresnel lens for formation of uniform light circle," *IEEE Photon. J.*, vol. 13, no. 3, Jun. 2021, Art. no. 2200108, doi: 10.1109/JPHOT.2021.3072538.

[18] M. L. Fu, E. E. Antonov, V. S. Lysenko, V. V. Petrov, and V. N. Zenin, "Uniform illumination of concentrated sunlight in photovoltaic solar modules with plane-focusing Fresnel lenses," *IEEE Photon. J.*, vol. 15, no. 4, Aug. 2023, Art. no. 5000310, doi: 10.1109/JPHOT.2023.3288155.

[19] E. E. Antonov, A. S. Lapchuk, V. V. Petrov, O. A. Tokalin, and V. N. Zenin, "Photodetector module of optoelectronic control systems for tracking the moving objects," *Semicond. Phys., Quantum Electron. Optoelectron.*, vol. 25, no. 3, pp. 315–322, 2022, doi: 10.15407/spqeo25.03.315.

[20] M. Born and E. Wolf, *Principles of Optics: Electromagnetic Theory of Propagation, Interference, and Diffraction of Light*. London, U.K.: Cambridge University Press, 1999.

[21] E. Brinksmeier, R. Glabe, and L. Schonemann, "Diamond micro chiseling of large-scale retroreflective arrays," *Precis. Eng.*, vol. 36, pp. 650–657, 2012, doi: 10.1016/j.precisioneng.2012.06.001.

[22] N. Y. Tan, D. W. K. Neo, X. Zhang, K. Liu, and A. S. Kumar, "Ultra-precision direct diamond shaping of functional micro features," *J. Manuf. Processes*, vol. 64, pp. 209–223, 2020, doi: 10.1016/j.jmapro.2020.12.064.

[23] Z. C. Le et al., "Anti-fatigue glasses based on microprisms for preventing eyestrain," *Sensors*, vol. 22, no. 5, pp. 1933–1948, 2022, doi: 10.3390/s22051933.

[24] V. Petrov, A. Kryuchyn, E. Antonov, A. Lapchuk, and S. Shanoylo, "Optical phenomena in microprism diagnostic set KK-42," *Proc. SPIE*, vol. 8011, 2011, Art. no. 80119A, doi: 10.1117/12.900751.

[25] N. Sultanova, S. Kasarova, and I. Nikolov, "Dispersion properties of optical polymers," *Acta Physica Polonica A*, vol. 116, pp. 585–587, 2009, doi: 10.12693/APhysPolA.116.585.

[26] A. B. Schroeder, E. T. A. Dobson, C. Rueden, P. Tomancák, F. Jug, and K. W. Eliceiri, "The imagej ecosystem: Open-source software for image visualization, processing, and analysis," *Protein Sci.*, vol. 30, no. 1, pp. 234–249, 2020, doi: 10.1002/pro.3993.

[27] Solidworks, 2020. [Online]. Available: http://www.solidworks.com

[28] J. Sarwar et al., "A novel configuration of a dual concentrated photovoltaic system: thermal, optical, and electrical performance analysis.," *Thermal Sci.*, vol. 27, pp. 2853–2863, 2023, doi: 10.2298/tsci220917209s.

[29] V. V. Petrov, E. E. Antonov, V. N. Zenin, M. Yu, and S. M. Shanoilo, "Peculiarities of forming homogenized images by plane-focusing fresnel lenses," *Data Recording, Storage Process.*, vol. 25, no. 1. pp. 3–21, 2023, doi: 10.35681/1560-9189.2023.25.1.286993.